A new scroll-type air motor with magnetic spirals

LUO, Xing, WANG, Jihong, SHPANIN, Leon <http://orcid.org/0000-0002-3085-4678> and DOONER, Mark

A New Scroll-Type Air Motor With Magnetic Spirals

Xing Luo, Jihong Wang, *Senior Member, IEEE*, Leonid Shpanin, *Member, IEEE*, and Mark Dooner

***Abstract*—The scroll-type air motor, also named the scroll expander, has been widely used for different applications due to its characteristics of compact structure and high energy conversion efficiency. However, the leakage and the friction result in non-negligible energy losses. This paper presents the recent work on developing a new scroll-type air motor with mounted permanent magnetic spirals and investigates its potential in leakage reduction and efficiency improvement, especially at low-pressure air supply conditions. A method for the implementation of the magnetic scroll air motor is proposed. A prototype is manufactured, and initial experimental tests are conducted to study the generalized torque distribution. A mathematical model for the magnetic scroll air motor is developed, and a corresponding simulation study is presented. The study shows that the proposed magnetic scroll air motor structure is feasible in terms of manufacturing and has the potential to reduce the air leakage and, thus, to improve the energy efficiency by a maximum of around 15% at a supply pressure of 2×10^5 Pa, with a flank leakage clearance reference of 0.06 mm.**

***Index Terms*—Energy efficiency, magnetic, mathematical modeling, prime mover of generator, scroll-type air motor.**

I. Introduction

PNEUMATIC motors convert compressed air energy into driving force for linear and angular motions, and their applications can be found in industrial and residential areas. The paper will focus on one particular type—the scroll-type air motor (also named the scroll expander), and it will propose a new design for improving its performance and energy efficiency.

The scroll technology has been widely applied in the compressors of air conditioners (e.g., residual and automotive air conditioning), refrigerators, and auxiliaries in different systems (e.g., superchargers for vehicle engines and some optical equipment) [1], [2]. The technology has recently been extended for manufacturing pneumatic motors (expanders) [3]–[5]. Inherited from the structure of scroll compressors, scroll-type air motors have distinguished merits, including compact design, operation reliability, low level of noise, and relatively high energy conversion ability at a certain range of working conditions [3]–[7].

The study of scroll-type air motors and scroll expansion equipment using different working mediums have been explored in both academia and industry, mainly focusing on the optimization study of the scroll geometry and the working process for improving the device's performance and efficiency, the applications of the scroll technology for recycling exhaust energy with low-pressure and/or low-grade heat characteristics, as a prime mover for electricity generators, and as a key energy conversion unit for small-scale energy storage through fuel cells and compressed air. A literature review of the recent progress on this area is presented later.

Concerning mathematical modeling and optimization, a mathematical description of a method to design a scroll-type air motor with variable wall thickness was developed by Wang *et al.* and Dickes in [8] and [9], respectively. An optimized volumetric (or expansion) ratio can be achieved by their developed models and the isentropic efficiency could be improved [8], [9]. A complete dynamic model for scroll air motors with validation was presented in [5]. The energy efficiency analysis was also performed, which explained the scroll's good ability in energy conversion [5]. The unsteady flow losses with vortexes in the suction process of the scroll expander have been studied via a three-dimensional transient computational fluid dynamic (CFD) numerical model, which can provide guidance for the optimal design of the suction port of scroll mechanism [10]. In the area of energy recovery, the performance of a scroll expander used for recovering the exhausted air from a fuel cell system was studied in [11]. The paper indicates that the leakage has a significant effect on the volumetric efficiency of the system. A hybrid pneumatic system that recovers energy from the exhaust air through a scroll expander was designed by Luo *et al.*, which concluded that, with a proper closed-loop coordinate control strategy, the energy efficiency improvement can reach 18.1% from the tests [12]. Luo *et al.* also studied a vehicle gasoline engine post-combustion mixture energy reusing system via the scroll technology [13]. The strategies for modification of the scroll expander were investigated and the simulation results indicated that it is possible to produce hundreds of Watts of power output from energy recycling, with over 90% of exhaust

Manuscript received February 13, 2017; revised July 18, 2017; accepted August 27, 2017. Date of publication November 17, 2017; date of current version February 14, 2018. Recommended by Technical Editor Y. Shtessel. This work was supported by the Engineering and Physical Sciences Research Council (EPSRC), U.K., under Grant EP/K002228/1 and Grant EP/L019469/1, and by the China 973 Research Programme under Grant 2015CB251301. *(Corresponding author: Jihong Wang.)*

X. Luo, J. Wang, and M. Dooner are with the School of Engineering, University of Warwick, Coventry, CV4 7AL, U.K. (e-mail: xing.luo@warwick.ac.uk; jihong.wang@warwick.ac.uk; M.Dooner.1@warwick.ac.uk).

L. Shpanin is with the Faculty of Engineering, Environment, and Computing, Coventry University, Coventry, CV1 5FB, U.K. (e-mail: leon.shpanin@coventry.ac.uk).

Color versions of one or more of the figures in this paper are available online at http://ieeexplore.ieee.org.

Digital Object Identifier 10.1109/TMECH.2017.2749378

flow being recycled [13]. The Organic Rankine Cycle (ORC) system is one of the most important application areas of scroll expanders. Song *et al.* reviewed the research in this area, including the prototypes of scroll expanders for ORC systems, theoretical modeling and CFD simulation in scroll machine design [7]. The leakage with clearances of scroll expanders is one of focuses in [7]. For small-scale Compressed Air Energy Storage (CAES) systems, Krupke *et al.* studied a scroll air motor within a small-scale CAES system to support wind power generation and integration [14]. The study demonstrates the benefit of improved efficiency with optimized tip speed ratio brought to the hybrid wind turbine operation [14].

In industry, the U.K.-based company Flowgroup (previously named FlowBattery and Energetix Group) commercialized the Compressed Air Battery (CAB) which can be considered as a variant of the small-scale CAES facility. It has been used in U.K. and U.S. national grids and data centers for uninterrupted power supply (UPS) [15]. The company has also released the micro combined heat and electrical power (CHP) system. It is claimed that people could save 20% of gas and electricity bills by using such type of CHP system at home [16]. The scroll air motor (expander) has been used as a core component in the two products for efficient multi-energy conversion [15], [16]. The US-based company Airsquared is a pioneer in the manufacture of scroll expanders [17]. The company has studied the combined scroll expansion–compression in hydrogen recirculation and many other scroll-relevant projects [17].

From the previous literature review, it can be found that, in many of the earlier designs/applications, scroll air motors (expanders) have been used as a prime mover to produce the driving torque for electrical generators [7], [12]–[17].

From the authors' previous study and the literature review, it is noticed that the energy conversion ability of scroll air motors is reduced when the supply air pressure is low [4], [5], [7], [11]. This is mainly caused by the air leakage between the chambers and the frictions. Such a characteristic will undoubtedly affect and limit many applications of scroll air motors, especially in low-pressure exhaust energy recycling and small-scale energy storage systems. To address this issue, the paper presents an innovative design by inserting permanent magnetic materials into the original fixed and moving scrolls to change the distribution of the acting forces/torques. It is expected that the developed magnetic scroll air motor has the potential to reduce the leakage and, in turn, improve the efficiency.

The paper begins with the description of the implementation of the proposed design. The magnetic field distribution and the flux density magnitude are studied via finite element simulation. An experimental study of the effect of the magnets is conducted using a prototype. A mathematical model for the design is then developed based on the model for ordinary scroll air motors. From the study, the potential benefits on the air leakage and the energy efficiency are justified.

II. Description of the New Magnetic Scroll

This section presents the principle of magnetic scroll air motors, the selection and the installation of magnetic materials, and the magnetization of magnetizable spiral segments.

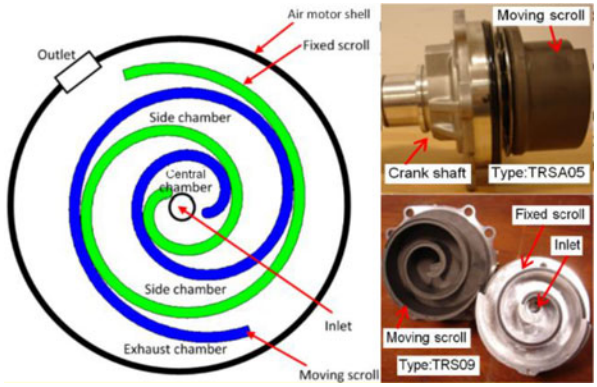

Fig. 1. Illustration of the ordinary scroll-type air motor structure [13] (modified from Sanden scroll compressors, types: TRSA05 and TRS09).

Fig. 1 shows the structures of two examples of ordinary scroll-type air motors. The main components of a scroll air motor consist of a moving scroll connected with a crank shaft via a bearing and a fixed scroll mounted inside a motor shell. From Fig. 1, it can be seen that the inlet port is at the center of the fixed scroll and the outlet port is located on the air motor shell. The compressed air flowing through the scroll air motor experiences three phases: 1) charging; 2) expansion; and 3) discharging, which associate with three types of chambers: a) central; b) side; and c) exhaust chambers, respectively [5]. When the compressed air goes through the three phases in the air motor, its pressure decreases and its energy is released and converted into the shaft kinetic energy in terms of the air motor driving torque output. The volumes of all chambers discontinuously vary in cycle-to-cycle operation. For details of scroll-type air motor operation, refer to [5] and [8].

In an ordinary scroll-type air motor, the material of both the fixed scroll and the moving scroll is a type of nonmagnetic alloy (see Fig. 1). For implementing the proposed design, two or more magnetic spiral segments are designed to be inserted into the two nonmagnetic alloy scrolls. Each magnetic spiral segment should be magnetized in a particular direction to enhance the air motor's useful torque output. In addition to the driving torque generated from the compressed air (which is the same as for ordinary scroll air motors), the magnetic field resulting from the magnetized spiral segments will generate extra workable torque at some angular positions and this extra torque can potentially benefit the air motor's operation and performance.

The selection of permanent magnetic materials is very important. The selection needs to consider the following important factors.

1) The selected materials must be able to produce a strong magnetic field to generate useful magnetic torque, which involves the consideration of key properties of magnetic materials, e.g., coercivity, the remanence of the permanent magnet, and energy density.
2) The magnetic materials should be able to operate and to provide a stable magnetic field within a wide temperature range, considering the various applications of the air motor, e.g., exhaust (heat) recovery.

From the study, the magnetic material chosen is Neodymium–Iron–Boron (NdFeB), which has a higher energy density than

TABLE I
COMPARISON OF PROPERTIES OF VACODYM 655 HR & 722 HR AT 20 °C [18]

Typical Values of Magnetic-Related Properties	VACODYM 655 HR	VACODYM 722 HR
Remanence B_r	1.28 T	1.47T
Energy density $(BH)_{\max}$	315 kJ/m^3	415 kJ/m^3
Coercivity H_{cB}	990 kA/m	915 kA/m
Inner magnetizing field strength H_{mag}	2500 kA/m	2500 kA/m
Maximum continuous temperature $T_{\max}$	150 °C	50 °C

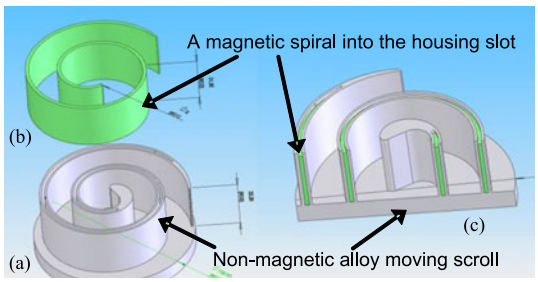

Fig. 2. Example of installing a single magnetic spiral into a housing slot of the nonmagnetic alloy moving scroll. (a) A non-magnetic alloy scroll envelope. (b) A magnetic spiral. (c) A magnetic spiral inserted into the slot of a non-magnetic alloy scroll envelope.

most other materials (the theoretical maximum energy density of NdFeB can be 485 kJ/m^3) [18]. From the category of NdFeB, the materials of VACODYM 655 HR and 722 HR (VACUUMSCHMELZE GmbH & Co. KG products) are considered as two options. The comparison of the properties of these two materials is given in Table I [18]. It is seen that VACODYM 722 HR has a higher energy density compared to VACODYM 655 HR; however, the maximum continuous temperature of VACODYM 655 HR is higher than that of VACODYM 722 HR. In addition, from the information of demagnetization and irreversible losses of these two materials at different temperatures (refer to [18]), VACODYM 722 HR can be more easily demagnetized compared to VACODYM 655 HR. Thus, VACODYM 655 HR is chosen for the prototype magnetic scroll air motor development.

To host the magnetic spiral segments, the mechanical modification of the existing air motor is considered. The two housing slots are machined on the original nonmagnetic alloy moving and fixed scrolls, respectively [an example is shown in Fig. 2(a)]. Magnetic spirals matching the shape and size of the slots are made [an example is shown in Fig. 2(b)], which are then inserted into the slots [see Fig. 2(c)]. Alternatively, multisegments of magnetized blocks can be inserted into each slot to make the design more flexible. Via this method, the original mechanical structure of the fixed and moving scrolls and the air flow route inside the air motor will not be affected; the nonmagnetic alloy scroll envelope [see Fig. 2(a)] provides mechanical support to the magnetic spirals. SolidWorks software is used for three-dimensional geometry structure design.

The method of magnetization of magnetizable spiral segments is important. The magnetic field strength generated from the magnetic spiral segments depends on the magnetizing directions and the magnetizing field strength. Thus, the positions of the magnetic poles of the magnetizable spiral segments are crucial. Also, to the different designs of configurations, the number of magnetized blocks and their magnetic poles can be different. This will be discussed further with the simulation study of the magnetic field distribution in the next section.

TABLE II
GEOMETRIC PARAMETERS OF THE PROTOTYPE MAGNETIC SCROLL AIR MOTOR

Parameters	Value
Slope of radius of curvature	0.003183
Effective inlet area	1.493×10^{-4} m^2
Effective outlet area	4.531×10^{-4} m^2
Orbit of the original moving scroll	5.8 mm
Thickness of each original nonmagnetic alloy scroll	4.5 mm
Height of each original nonmagnetic alloy scroll	33.3 mm
Thickness of each magnetic spiral	2.0 mm
Height of each magnetic spiral	31.5 mm

III. SIMULATION STUDY OF MAGNETIC FIELD AND FLUX DENSITY OF THE MAGNETIC SCROLL AIR MOTOR

For the simulation study and the prototype development, the geometric parameters of the scroll air motor used are listed in Table II, which are based on the structure of a Sanden scroll compressor (Type: TRS09, Fig. 1).

The magnetic field distribution variation is dependent on the relative positions of the magnetic spiral segments, which is determined by the instant position of the moving scroll, which moves along its orbit angles. Specifically, because the moving scroll's orbit angle decides its location and its movement repeats cycle by cycle, the variation trends of the magnetic field distribution and the generalized force/torque resulting from the permanent magnets' induced magnetic field are periodically repeated in each cycle without control. For every relative position of the magnetic spiral segments, a steady magnetic field analysis is carried out. The ANSYS Maxwell software is employed for the magnetic field distribution simulation. In the Maxwell simulation settings, the magnetostatic solver is chosen for the simulation of the magnetic field distribution and flux density magnitude, the default boundary condition (Natural and Neumann) is used, and the source of the static magnetic field are permanent magnets with the material NdFeB chosen.

Two simulation cases corresponding to two topologies of the magnetic spiral segments are studied, that is, Case I and Case II. The simulation cases help to understand how the different magnetic fields with flux densities can be generated from the different configurations of magnet material insertion patterns.

Fig. 3 shows the magnetic field distribution with the flux density magnitude simulation results for Case I, that is, one magnetizable spiral is inserted into the housing slot of the nonmagnetic alloy moving scroll (refer to Fig. 2) and another is inserted into the slot of the nonmagnetic alloy fixed scroll. Fig. 3(a) and (b) presents the simulation results of the magnetic field distribution with the flux density, when the relative positions of the two nonmagnetic alloy scrolls are at two specific orbit angles (0° and 90°). Fig. 3(c) presents the magnetic flux density distribution of the moving scroll in three dimensions. The magnetization direction of the magnetizable spiral mounted on the moving scroll is

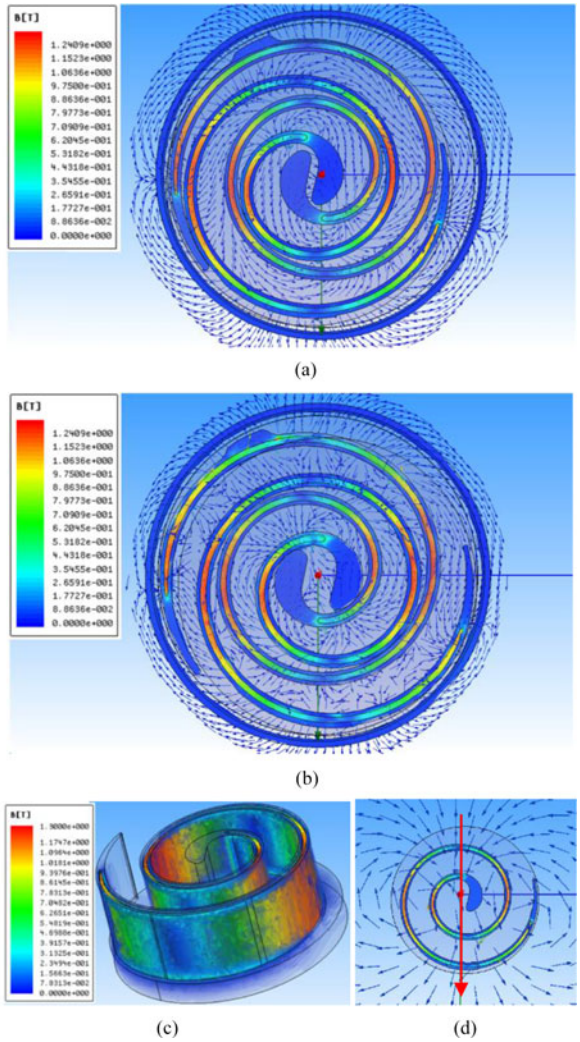

Fig. 3. Simulation results for the magnetic field distribution and the flux density magnitude (Case I: single magnetic spiral in each housing slot) [19]. (a) Magnetic field distribution and flux density magnitude (the orbit angle 0°). (b) Magnetic field distribution and flux density magnitude (the orbit angle 90°). (c) Flux density magnitude. (d) Magnetization direction.

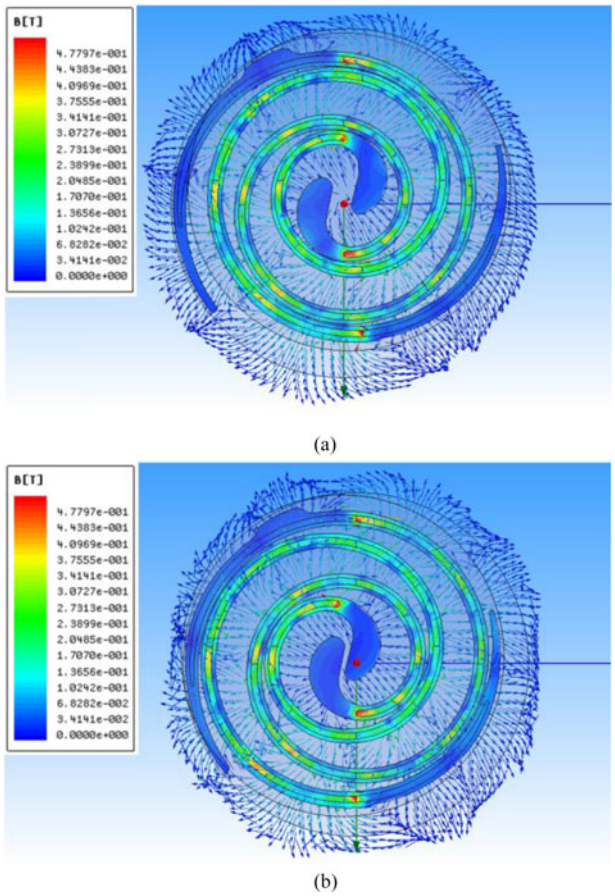

Fig. 4. Simulation results for the magnetic field distribution and the flux density magnitude (Case II: multi magnetic spiral blocks in each housing slot). (a) Magnetic field distribution and flux density magnitude (the orbit angle 180°). (b) Magnetic field distribution and flux density magnitude (the orbit angle 270°).

shown in Fig. 3(d) ("red arrow") and the magnetization direction for the magnetizable spiral on the fixed scroll is opposite to this direction.

Fig. 4 presents the simulation results from Case II, that is, 12 piecewise magnetic segments are inserted into each housing slot, and thus, there are 24 magnetic blocks in total. Fig. 4(a) and (b) presents the magnetic field distribution with the flux density, while the positions of the nonmagnetic alloy moving scrolls are at the orbit angles of 180° and 270°, respectively. The magnetization directions of these magnetic blocks are alternately directed toward or away from the origin of coordinates; adjacent magnetic blocks, which are located in the different housing slots, are magnetized in opposite directions.

From the simulation study of Cases I and II, it is found that the relative positions of two scrolls in Case I has a greater effect on the magnetic field distribution than Case II. From the comparison of Fig. 3(a) and (b), it can be seen that for Case I, the magnetic field distribution changes in dependence with the moving scroll's orbital position: the turbulence marked by blue arrows can be observed in Fig. 3(b). Conversely, from the comparison of Fig. 4(a) and (b), the magnetic field distribution for Case II is not obviously affected by the relative positions. Thus, the periodic variations of magnetic force and torque resulting from the magnetic field distribution in Case II should be smoother in cycle-to-cycle operation compared to Case I. Less vibration could lead to a stable mechanical torque output from the air motor and in turn to possibly deliver electricity with high power quality if the magnetic scroll device is coupled with an electrical generator.

IV. Experimental Tests of Torques of the Prototype Magnetic Scroll Air Motor

A prototype magnetic scroll air motor with a single magnetic spiral mounted in each housing slot (Fig. 2 and also Case I in Section III) was recently developed at Warwick. The prototype is originally modified from a Sanden scroll compressor (Type: TRS09). Its geometric parameters are given in Table II. The installation of magnetic material (VACODYM 655 HR) and the magnetization was made by VACUUMSCHMELZE GmbH & Co. KG.

Fig. 5 illustrates the magnetic field distribution of the prototype scroll with the mounted magnetized spiral. The patterns

Fig. 5. Illustration of the manufactured prototype magnetic scroll air motor (N: North Pole; S: South Pole) [19].

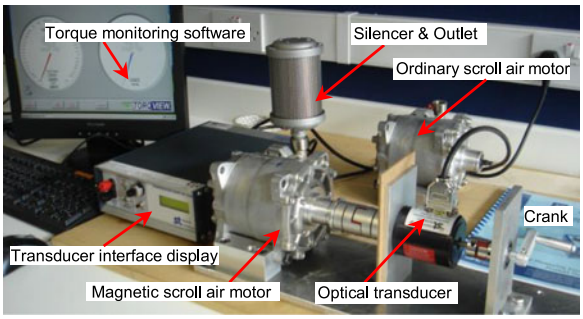

Fig. 6. Experimental test rig for the prototype magnetic scroll air motor.

in Fig. 5 are generated by placing iron powder on the top of the scroll with the magnetized spiral. From Fig. 5, the magnetic field distribution from the prototype is visualized to aid understanding the magnetic field distribution simulation result (see Fig. 3).

A test rig is set up at the authors' research laboratory to measure the torque resulting from the prototype and to observe the performance difference between the prototype and an ordinary scroll air motor TRS09 with the same structure. The experimental test rig is presented in Fig. 6. The shaft of the prototype magnetic scroll air motor is connected to an optical rotary transducer (Type: E200-ORT-06, Sensor Technology Ltd.) via one pair of mechanical couplings. The transducer is also connected to a crank as shown in Fig. 6 and is used to measure the torque from the prototype shaft. The measured output of the transducer is stored via an optical torque interface with its software, Torqview.

The experimental tests were implemented as follows. Both the ordinary scroll air motor without magnetized materials and the prototype magnetic scroll air motor are assembled by the specialist from the U.K.-based company, Flowgroup Ltd., which is to ensure the friction distribution from the shell assembly is as even as possible for both scroll air motors. In the tests, the required torques for starting the rotor rotation at different angle positions of both scroll air motors are measured individually via turning the crank to adjust the angle position of the shaft, which is associated with the relative (angle) positions of the moving and fixed scrolls. The measurement of the torques was taken every ten degrees.

Fig. 7 shows the experimental test results of the starting rotation torques for the ordinary scroll air motor and the prototype respectively. In Fig. 7, it can be seen that: for the ordinary scroll air motor without magnetized materials, the variation range of the torque for starting rotation in one cycle is within 0.977 ± 9.5% N·m (the red solid line) and its average value is 0.977 N·m

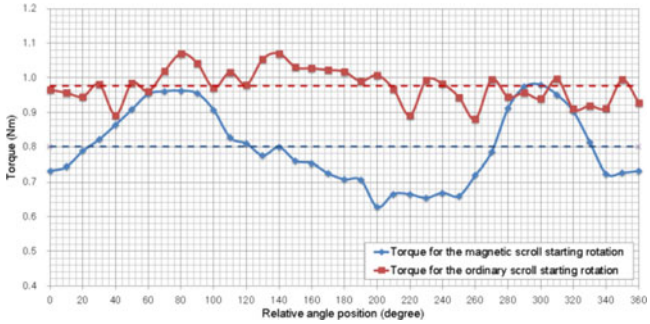

Fig. 7. Experimental results for the torques for starting rotations of the ordinary scroll air motor and the prototype magnetic scroll air motor.

(the red dotted line); for the prototype magnetic scroll air motor, the variation range of the corresponding torque is within 0.801 ± 22.9% N·m (the blue solid line in Fig. 7, named $\tau_{\mathrm{mag\_start}}$) and its average value is 0.801 N·m (the blue dotted line). It is clear that the variation range of the measured torque of the prototype magnetic scroll air motor is wider than that of the ordinary scroll air motor. The test data from the prototype indicates the combined effect of the magnetic torque generated from the magnetic field and the torque resulting from the maximum mechanical static friction, while the measurement data from the ordinary scroll air motor shows the effect from the maximum mechanical static friction only. Thus, the trends and ranges of the two solid line curves in Fig. 7 are different; with the magnetic torque involved, the performance of the scroll mechanism is changed. Considering the measurement data from the prototype tests, the starting rotation torque is required to overcome the resisting moment due to the maximum mechanical static friction, which is assumed to be a constant of 0.801 N·m (assuming the maximum mechanical static friction is evenly distributed, refer to [20]–[22]). Then the magnetic torque can be expressed as

$$\tau_{\mathrm{magnet}} = \tau_{\mathrm{mag\_start}} - 0.801, \quad \tau_{\mathrm{magnet}} \in [-0.172,\ 0.177] \tag{1}$$

where τ_{magnet} is the resultant magnetic torque from the induced field of magnetized spirals.

V. Mathematical Modeling of a Magnetic Scroll Air Motor and Further Simulation Study

A. Mathematical Modeling

This subsection presents the mathematical modeling of the magnetic scroll air motor, which starts from the modeling descriptions of the ordinary scroll air motor without mounted permanent magnets.

The geometry description of the ordinary scroll air motor is based on the geometry for scroll compressors ([23]) and the details were reported in [8]. The mathematical descriptions for the moving scroll $A(\varphi_s, \alpha_s)$ are

$$x_{\mathbf{A}}(\varphi_s, \alpha_s) = x_0 + (\rho_0 + k\varphi_s)\sin\varphi_s + k\cos\varphi_s - k + r_s\sin\alpha_s \tag{2a}$$

$$y_{\mathbf{A}}(\varphi_s, \alpha_s) = y_0 - (\rho_0 + k\varphi_s)\cos\varphi_s + k\sin\varphi_s + \rho_0 - r_s\cos\alpha_s \tag{2b}$$

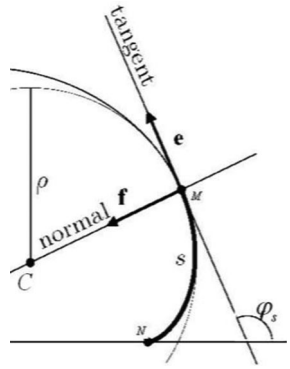

Fig. 8. Geometry of a moving scroll spiral.

with the orbit of the moving scroll

$$\vec{\mathrm{D}} = r_s\,(\sin\alpha_s, -\cos\alpha_s)$$

where k is the slope of radius of curvature, determining the shape of a scroll spiral; ρ_0 is the initial radius of the curvature, $\rho = \rho_0 + k\varphi_s$; (x_0, y_0) is the initial point of the moving scroll; φ_s is the tangential angle of a point on a moving scroll; α_s is the orbit angle of the moving scroll; and r_s is the radius of the orbit. Fig. 8 shows the geometry of a moving scroll spiral. The corresponding fixed scroll $B(\phi_s)$ is described as (see [14] and [15])

$$x_{\mathrm{B}}(\phi_s) = x_1 + (\rho_0 + k\phi_s)\sin\phi_s + k\cos\phi_s - k \tag{3a}$$

$$y_{\mathrm{B}}(\phi_s) = y_1 - (\rho_0 + k\phi_s)\cos\phi_s + k\sin\phi_s + \rho_0 \tag{3b}$$

where (x_1, y_1) is the initial point of the fixed scroll and ϕ_s is the tangential angle of a point on a fixed scroll.

Based on the validated model for ordinary scroll air motors (refer to [5], [8]), the model for the prototype magnetic scroll air motor, with consideration of the air leakage, can be described. For mathematical modeling, the following assumptions are made: 1) the gas used for driving the scroll air motor is an ideal gas and the gas is uniformly distributed in each chamber; 2) during the scroll air motor operation, the heat transfer between different chambers and heat transfer to the outside of the air motor is neglected (refer to [5] and [8]).

For the central chamber of magnetic scroll air motors

$$\begin{aligned} V_{s\_c}(\alpha_s) = z\Big[&\left(kr_s - k^2\pi - x_0 r_s + x_0 k\pi\right)\cos\alpha_s \\ &- \frac{1}{2}kr_s\pi^2 + \rho_0 r_s\pi + (kr_s\rho_0\pi - r_s\rho_0 - y_0 r_s \\ &+ y_0 k\pi)\sin\alpha_s + \frac{1}{2}{r_s}^2\pi + \rho_0^2\pi + (kr_s\pi \\ &+ 2k\rho_0\pi)\alpha_s + k^2\pi{\alpha_s}^2 - kr_s + \frac{1}{3}k^2\pi^3\Big] \end{aligned} \tag{4}$$

$$\begin{aligned} \dot{T}_{s\_c} = \frac{1}{[X_{\mathrm{air}}]C_{p,\mathrm{air}}(T_{s\_c}) - \frac{P_{s\_c}}{T_{s\_c}}}\Bigg\{&\frac{\dot{m}_{\mathrm{in}}h_{\mathrm{in}}}{V_{s\_c}} - \frac{\dot{m}_{\mathrm{leak}c\_s}h_{s\_c}}{V_{s\_c}} \\ &- \frac{\dot{V}_{s\_c}}{V_{s\_c}}[X_{\mathrm{air}}]\hat{h}_{s\_c} - [\dot{X}_{\mathrm{air}}]\hat{h}_{s\_c} + \frac{P_{s\_c}[\dot{X}_{\mathrm{air}}]}{[X_{\mathrm{air}}]}\Bigg\} \end{aligned} \tag{5}$$

$$\dot{P}_{s\_c} = \frac{1}{V_{s\_c}}\left(\frac{\dot{m}_{s\_c}}{M_{\mathrm{air}}}RT_{s\_c} + R\dot{T}_{s\_c}\frac{m_{s\_c}}{M_{\mathrm{air}}} - P_{s\_c}\dot{V}_{s\_c}\right). \tag{6}$$

For the side chamber of magnetic scroll air motors

$$V_{s\_s}(\alpha_s, n) = z\left\{\pi {r_s}^2 + 2\pi r_s[\rho_0 + k(\alpha_s + \pi + 2(n-1)\pi)]\right\} \quad (n = 1, 2, \ldots) \tag{7}$$

$$\begin{aligned} \dot{T}_{s\_c} = \frac{1}{[X_{\mathrm{air}}]C_{p,\mathrm{air}}(T_{s\_s}) - \frac{P_{s\_s}}{T_{s\_s}}}\Bigg\{&\frac{\dot{m}_{\mathrm{leak}c\_s}h_{s\_c}}{V_{s\_s}} - \frac{\dot{m}_{\mathrm{leak}s\_e}h_{s\_s}}{V_{s\_s}} \\ &- \frac{\dot{V}_{s\_s}}{V_{s\_s}}[X_{\mathrm{air}}]\hat{h}_{s\_s} - [\dot{X}_{\mathrm{air}}]\hat{h}_{s\_s} + \frac{P_{s\_s}[\dot{X}_{\mathrm{air}}]}{[X_{\mathrm{air}}]}\Bigg\} \end{aligned} \tag{8}$$

$$\dot{P}_{s\_s} = \frac{1}{V_{s\_s}}\left(\frac{\dot{m}_{s\_s}}{M_{\mathrm{air}}}RT_{s\_s} + R\dot{T}_{s\_s}\frac{m_{s\_s}}{M_{\mathrm{air}}} - P_{s\_s}\dot{V}_{s\_s}\right). \tag{9}$$

For the exhaust chamber of magnetic scroll air motors

$$V_{s\_e}(\alpha_s) = V_{s\mathrm{total}} - V_{s\_c}(\alpha_s) - \sum V_{s\_s}(\alpha_s, n), \quad (n = 1, 2, \ldots) \tag{10}$$

$$\begin{aligned} \dot{T}_{s\_e} = \frac{1}{[X_{\mathrm{air}}]C_{p,\mathrm{air}}(T_{s\_e}) - \frac{P_{s\_e}}{T_{s\_e}}}\Bigg\{&\frac{\dot{m}_{\mathrm{leak}s\_e}h_{s\_s}}{V_{s\_e}} - \frac{\dot{m}_{\mathrm{out}}h_{s\_e}}{V_{s\_e}} \\ &- \frac{\dot{V}_{s\_e}}{V_{s\_e}}[X_{\mathrm{air}}]\hat{h}_{s\_e} - [\dot{X}_{\mathrm{air}}]\hat{h}_{s\_e} + \frac{P_{s\_e}[\dot{X}_{\mathrm{air}}]}{[X_{\mathrm{air}}]}\Bigg\} \end{aligned} \tag{11}$$

$$\dot{P}_{s\_e} = \frac{1}{V_{s\_e}}\left(\frac{\dot{m}_{s\_e}}{M_{\mathrm{air}}}RT_{s\_e} + R\dot{T}_{s\_e}\frac{m_{s\_e}}{M_{\mathrm{air}}} - P_{s\_e}\dot{V}_{s\_e}\right) \tag{12}$$

where the subscripts s_c, s_s, s_e represent the central, side, and exhaust chambers of scroll-type air motors, respectively; the subscripts in, out refer to the inlet and outlet, respectively; V stands for control volume; $V_{s\mathrm{total}}$ is the total control volume of the air motor; T represents the temperature inside the chambers; P stands for pressure; R is the universal gas constant; z is the height of the scroll wall; n is the number of pairs of side chambers; $\dot{m}$ is the mass flow rate; M_{air} is the molar mass of air; h is the enthalpy of air; $\hat{h}$ is the specific enthalpy of air on a molar basis; $[X_{\mathrm{air}}]$ is the molar volumetric concentration of air; $C_{p,\mathrm{air}}$ is the specific heat of air; $\dot{m}_{\mathrm{leak}c\_s}$ is the leakage mass flow rate from the central chamber to the side chambers; and $\dot{m}_{\mathrm{leak}s\_e}$ is the leakage mass flow rate from the side chambers to the exhaust chamber. The driving torque (τ_{s_air}) generated from compressed air energy is

$$\begin{aligned} \tau_{s\_\mathrm{air}}(P_{s\_c}, P_{s\_s}, P_{s\_e}) &= r_s F_{s\_\mathrm{air}}(P_{s\_c}, P_{s\_s}, P_{s\_e}) \\ &= r_s \sum_{j=0,1,2,\ldots}[z\hat{P}(P_{s\_c}, P_{s\_s}, P_{s\_e}) \\ &\quad \times (2\rho_0 + 2k\alpha_s + (4j+1)\,k\pi)] \end{aligned} \tag{13}$$

where $F_{s\_air}(P_{s\_c}, P_{s\_s}, P_{s\_e})$ represents the driving force generated from compressed air and $\hat{P}(P_{s\_c}, P_{s\_s}, P_{s\_e})$ is the pressure difference between the adjacent chambers (refer to [5] and [8]). The above is the modeling descriptions of the ordinary scroll air motor, based on its "geometry and the fundamentals of thermodynamics and rotary motion." Considering the magnetic torque generated from the induced magnetic field, the shaft acceleration $(\dot{\omega}_s)$ of a magnetic scroll air motor is given by

$$\dot{\omega}_s = \frac{1}{J_s}[-K_{S-C}S(\omega_s, P_{s\_c}, P_{s\_s}, P_{s\_e}) - K_{fs}\omega_s - T_l + \tau_{s\_air}(P_{s\_c}, P_{s\_s}, P_{s\_e}) + \tau_{\text{magnet}}] \tag{14}$$

where T_l is the air motor load torque; the maximum of j is determined by the number of the driving segments of scrolls; ω_s and $\dot{\omega}_s$ represent the rotor rotating angular speed and acceleration; J_s is the air motor inertia; K_{fs} is the coefficient of kinematic viscous friction; $K_{S-C}S(\omega_s, P_{s\_c}, P_{s\_s}, P_{s\_e})$ is the combination effect on torque resulting from the static plus Coulomb frictions with the consideration of the effect from the magnetic force, which can be described as

$$K_{S-C}S(\omega_s, P_{s\_c}, P_{s\_s}, P_{s\_e}) = \begin{cases} K_{S-C}F_{\text{mag\_staticmax}}, & \omega_s = 0 \\ \text{sign}(\omega_s) \times \partial_s \times K_{S-C}F_{\text{mag\_staticmax}}, & \omega_s \neq 0 \end{cases} \tag{15}$$

where K_{S-C} is a coefficient of this combination effect; ∂_s is the coefficient for the Coulomb friction, $0 < \partial_s < 1$; $K_{S-C}F_{\text{mag\_staticmax}}$ is the combined effect on torque from the magnetic force and the maximum mechanical static friction.

From the fundaments of magnetics, the magnetic torque generated by the magnetic field can be defined as (see [24]–[26])

$$\begin{aligned} \tau_{\text{magnet}} &= \vec{r}_s\vec{F}_{\text{magnet}} = r_sF_{\text{magnet}} \times \cos\theta = r_s\cos\theta \times \left[-\frac{d}{d\tilde{x}}(W_a + W_m)\right] \\ &= r_s\cos\theta \times \left[-\frac{d}{d\tilde{x}}\left(\int_{\text{vola}}\left(\int_0^B \vec{H}_a d\vec{B}_a\right)dv_a + \int_{\text{volm}}\left(\int_{B_r}^B \vec{H}_m d\vec{B}_m\right)dv_m\right)\right] \end{aligned} \tag{16}$$

where θ is the angle between the directions of the moving scroll movement and the resultant magnetic force; F_{magnet} is the resultant force on the magnet(s); $\tilde{x}$ represents the object position; W_a is the energy in an air medium (e.g., a chamber) with the magnetic flux density $(\vec{B}_a)$ and the magnetic field strength $(\vec{H}_a)$; vola and dv_a are, respectively, the volume of the air field and the volume of its segment; W_m is the energy in a magnet block with the magnetic flux density $(\vec{B}_m)$ and the magnetic field strength $(\vec{H}_m)$; volm and dv_m are, respectively, the volume of magnet block and the volume of its segment.

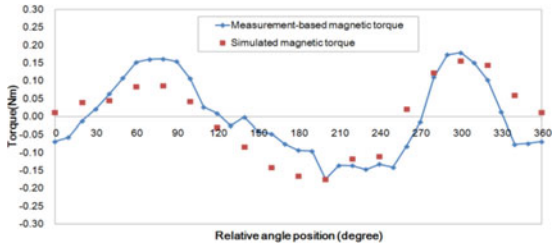

Fig. 9. Comparison of measurement-based and simulated magnetic torques.

B. Simulation Study

The simulation study is implemented via using the developed model in ANSYS Maxwell with MathWorks MATLAB, the overall variation trend of the magnetic torque from the simulated results is roughly comparable to the measurement-based data (τ_{magnet} from (1) in Section IV). The comparison is shown in Fig. 9, from which it can be seen that there are some differences between the simulated results and the measurement-based data. This difference is mainly caused by the assumption made for mechanical static friction which is used in the calculation of τ_{magnet}. It is assumed that the maximum mechanical static friction is evenly distributed. But, in practice, it varies with the different orbit angles (α_s). One case is shown in Fig. 7 (the red solid line): the starting torque for the ordinary scroll air motor without magnets is unevenly distributed which is due to the varied maximum mechanical static friction with orbit angles.

For the magnetic scroll air motor, the resultant magnetic force/torque can affect the clearances between the moving and fixed scrolls, in turn the air leakage of the scroll air motor. There are two types of leakages associated with the air motor operation, i.e., flank and radial leakages (refer to [5]). Based on the current prototype design, the magnetic force/torque can only vary the flank leakage during the operation. The mass flow rate of the flank leakage is [5] given by (17) as shown at the bottom of this page, where a_r is leakage flow coefficient; γ is specific heat ratio of air, $\gamma \approx 1.4$; ρ is the compressed air density; subscript i stands for the ith pair of side chambers; and δ_f is the flank gap clearance, which can be assumed to be a constant, for ordinary scroll air motors $\delta_f \approx 0.01 - 0.06$ mm [5], [7], [11], [27], [28]. From (17), the quantity of air leakage changes with the variation of clearance δ_f, which is affected by the magnetic force/torque. Due to the difficulties in measuring the leakage and the magnetic force during the air motor operation, the investigation of leakage effect with efficiency analysis is performed via simulation study. It is assumed that

$$\dot{m}_{\text{flank}} = \begin{cases} 2a_r z\delta_f\rho_i\sqrt{\frac{2\gamma}{\gamma-1}RT_i\left[\left(\frac{P_{i+1}}{P_i}\right)^{2/\gamma} - \left(\frac{P_{i+1}}{P_i}\right)^{(\gamma+1)/\gamma}\right]} & \text{(unchoked)} \\ 2a_r z\delta_f\rho_i\sqrt{\frac{2\gamma}{\gamma-1}RT_i\left[\left(\frac{2}{\gamma+1}\right)^{(2/\gamma-1)} - \left(\frac{2}{\gamma+1}\right)^{(\gamma+1)/(\gamma-1)}\right]} & \text{(choked)} \end{cases} \tag{17}$$

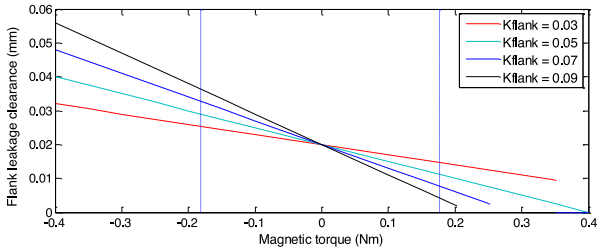

Fig. 10. Relationship between magnetic torque and flank leakage clearance.

the prototype magnetic torque can linearly affect the flank leakage clearance, i.e., $\delta_f = \delta_{f\_\mathrm{ini}} - K_{\mathrm{flank}}\tau_{\mathrm{magnet}}(\delta_f \geq 0)$, δ_{f_ini} is the initial value of the flank leakage clearance, which can be chosen from 0.01 to 0.06 mm, according to the range of the flank leakage clearance for ordinary scroll air motors (refer to [5], [7], [11], [27], and [28]); K_{flank} is a coefficient and its range needs to consider the value of τ_{magnet}. Based on the above assumption relevant to the linear effect generated from the magnetic torque to the flank leakage clearance, Fig. 10 shows the relationship between the magnetic torque and the flank leakage gap clearance with different values of K_{flank} when $\delta_{f\_\mathrm{ini}} = 0.02$ mm. A larger value of K_{flank} will impose a greater effect on the leakage clearance. In the study, τ_{magnet} is from -0.172 to 0.177 N·m [see (1)] and thus $K_{\mathrm{flank}} \in [0,\ 0.113]$.

To study how the magnetic force/torque influences the effect of air leakage in scrolls, the rate of flank leakage amount is defined as

$$\lambda_{\mathrm{flank\_leakage}} = \frac{\hat{m}_{\mathrm{flank\_down}}}{\hat{m}_{\mathrm{in}}} \times 100\% \qquad (18)$$

where $\hat{m}_{\mathrm{in}}$ is the air mass which is from the air motor inlet to the central chamber in steady state operation, with the duration corresponding to the orbit angle rotation from 0° to α_s, $\alpha_s \in [0°, 360°)$; $\hat{m}_{\mathrm{flank\_down}}$ is the air mass resulting from flank leakage at the steady states, which is from the central chamber to the downstream chambers, with the same duration as $\hat{m}_{\mathrm{in}}$. The rate of flank leakage amount ($\lambda_{\mathrm{flank\_leakage}}$) indicates how much influence the flank leakage has on the scroll machine operation during steady states.

Fig. 11 shows the simulation results of the rate of flank leakage amount with $\delta_{f\_\mathrm{ini}} = 0.02$ mm, including the comparison of the rates between the ordinary scroll air motor and the prototype magnetic scroll air motor [see Fig. 11(a)], and the rates of flank leakage amount of the prototype with the different values of K_{flank} [see Fig. 11(b)]. The parameters used for the simulation study are listed in Table II. The measurement-based magnetic torque is used for the simulation, which is implemented via a look-up table. From Fig. 11(a), with K_{flank} keeping at a constant value of 0.0565, a comparison of the different supply pressures can be seen. It is seen that, the lower the supply pressures, the grater the effect of air leakage on both the ordinary and magnetic scroll air motors. Also, the effect of magnetic torque on the rate $\lambda_{\mathrm{flank\_leakage}}$ is more obvious at the lower supply pressures. Thus, the applications of magnetic scroll air motors should be more valuable in the low air pressure operation conditions, e.g., exhaust energy recycling. According to this, Fig. 11(b) studies the rate of flank leakage amount at a low supply pressure

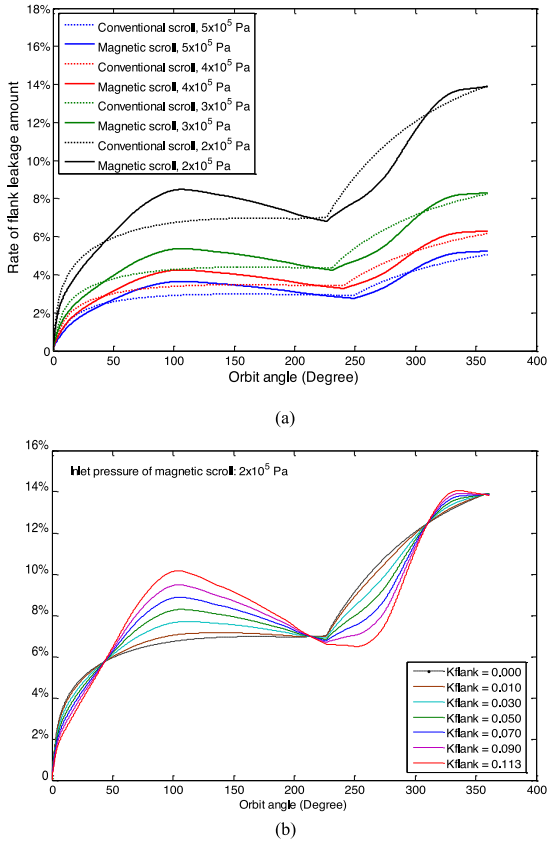

Fig. 11. Simulation results for the rate of flank leakage amount ($\delta_{f\_\mathrm{ini}} = 0.02$ mm). (a) Comparison of the rates of flank leakage amount between the ordinary scroll TRS09 and the prototype magnetic scroll ($\delta_{f\_\mathrm{ini}} = 0.02$ mm, $K_{\mathrm{flank}} = 0.0565$). (b) The rates of flank leakage amount of the prototype magnetic scroll air motor with the different values of K_{flank} ($\delta_{f\_\mathrm{ini}} = 0.02$ mm).

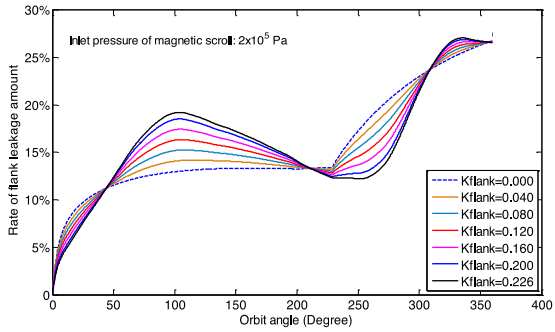

Fig. 12. Simulation results for the rate of flank leakage amount of the prototype magnetic scroll air motor ($\delta_{f\_\mathrm{ini}} = 0.04$ mm).

2×10^5 Pa with $\delta_{f\_\mathrm{ini}} = 0.02$ mm and the different values of K_{flank} are used ($K_{\mathrm{flank}} \in [0,\ 0.113]$). The dotted line ($K_{\mathrm{flank}} = 0$) shows the rate $\lambda_{\mathrm{flank\_leakage}}$ of the ordinary scroll air motor. For comparison, Fig. 12 shows the simulation results for the rate of leakage amount at 2×10^5 Pa with $\delta_{f\_\mathrm{ini}} = 0.04$ mm. In this case, considering $\delta_f = \delta_{f\_\mathrm{ini}} - K_{\mathrm{flank}}\tau_{\mathrm{magnet}}$ ($\delta_f \geq 0$), $K_{\mathrm{flank}} \in [0,0.226]$, because of the increase of the initial value of the flank clearance (δ_{f_ini}). It can be seen that, the amplitude variation of the rate of flank leakage amount in Fig. 12 can be higher than that in Fig. 11(b). Thus, the potential of the reduction of air leakage in Fig. 12 could be more obvious

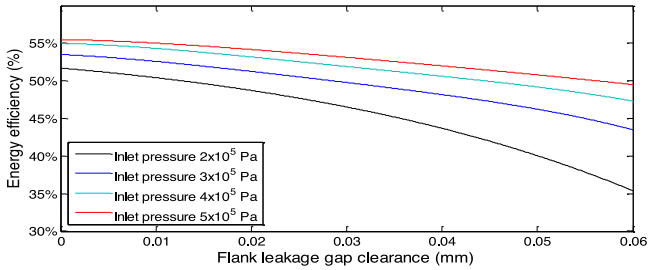

Fig. 13. Simulation results of flank leakage clearance versus energy efficiency.

compared to the results shown in Fig. 11(b). This indicates that the potential of the reduction of air leakage not only depends on the strength of magnetic force/torque but also the initial original air leakage with its clearance.

The available air power at the inlet can be defined as the maximum potential power that can be extracted from the compressed air [29]

$$\tilde{P}_{\text{airin}} = \dot{m}_{\text{in}}[(h_{\text{in}} - h_{\text{atm}}) - T_{\text{atm}}(s_{\text{in}} - s_{\text{atm}})] \tag{19}$$

where subscripts in and atm are the inlet and atmospheric states of the compressed air, respectively; s is the specific entropy of air. From the fundamentals of thermodynamics, an alternative for calculating the air power can be [29]–[31]

$$\tilde{P}_{\text{airin}} = \dot{m}_{\text{in}} R_{\text{air}} T_{\text{atm}} \times \left[\ln \frac{P_{\text{in}}}{P_{\text{atm}}} + \frac{\gamma}{\gamma - 1}\left(\frac{T_{\text{in}}}{T_{\text{atm}}} - 1 - \ln \frac{T_{\text{in}}}{T_{\text{atm}}}\right)\right] \tag{20}$$

where R_{air} is the gas constant for air. The energy efficiency of the magnetic scroll air motor can be defined as

$$\eta = \frac{\tilde{P}_{\text{mag\_scroll}}}{\tilde{P}_{\text{airin}}} = \frac{\omega_s}{\tilde{P}_{\text{airin}}}[\tau_{s\_\text{air}}(P_{s\_c}, P_{s\_s}, P_{s\_e}) + \tau_{\text{magnet}} - K_{S-C} S(\omega_s, P_{s\_c}, P_{s\_s}, P_{s\_e}) - K_{fs}\omega_s] \tag{21}$$

where $\tilde{P}_{\text{mag\_scroll}}$ is the generated net power from the shaft of the magnetic scroll air motor. Fig. 13 shows the simulation results of the change of energy efficiency of the magnetic scroll air motor with the flank leakage clearance variation. In the simulation study, the clearance causing the radial leakage is set as a constant of 0.015 mm, and the radial leakage calculation is similar to the flank leakage (for details, refer to [5] and [28]). In Fig. 13, when the supply inlet pressure is at 2×10^5 Pa, with the assumption that the original flank leakage clearance is 0.02 mm, the energy efficiency can be maximally improved by about 4.0% (considering the flank leakage clearance can be reduced to 0); the potential of efficiency improvement can be up to around 8.3%, when the original value of the flank clearance $\delta_{f\_\text{ini}} = 0.04$ mm; the energy efficiency has the possibility to improve around 15% if $\delta_{f\_\text{ini}} = 0.06$ mm.

C. Further Discussion

The simulation study reported in this section shows the relationship between the magnetic torque, the flank leakage, and the energy efficiency of the magnetic scroll air motor. Figs. 11 and 12 indicate that the current magnetization strategy for the prototype magnetic scroll can reduce the air leakage only in some sections but not the whole cycle. This gives important information in developing a better strategy for the design of magnetic scroll air motors. It can be considered that using electromagnets to replace some of the permanent magnets to be inserted into the scroll air motor would allow the generated magnetic torque to be controlled by the supplied excitation current into the windings wrapped around the electromagnets. This will optimize the sections of air leakage reduction in each cycle operation. The research to the new strategy is currently on-going work within the research group.

VI. Conclusion

An innovative scroll-type air motor with magnetized spirals is proposed in the paper. The realization of the magnetic scroll concept is explored and a feasible technique is proposed, that is, machining two thin slots on both fixed and moving scrolls to host the magnetized spiral segments. A prototype of the magnetic scroll air motor is manufactured, which proves the feasibility. The technique proposed retains the original mechanical structure for airflow and also protects the embedded magnetic materials.

The simulation study on two different topologies of embedding magnetic spiral segments inside the air motor enhances the understanding of the corresponding magnetic fields and the flux density distributions. This can provide a guide for optimizing magnetization of the scrolls. The effect of the magnetization and the generated magnetic torque on the scroll air motor performance and operation is studied via modeling, simulation, and experiment.

From the study, it can be concluded that: the magnetized spirals will result in additional torques and their directions depend on the direction of magnetization; the developed magnetic scroll air motor has potential in reducing the leakage between air chambers and, in turn, improving the energy efficiency. The study shows that it has potential to improve efficiency by around 15% at 2×10^5 Pa supply pressure condition with the initial flank clearance at 0.06 mm. This opens a wider opportunity for scroll technology to be used in the applications with low air pressure operation conditions, such as exhaust energy recycling.

Acknowledgment

The authors would like to thank the Engineering and Physical Sciences Research Council (EPSRC) for the funding support and the China 973 Research Programme to enable the U.K.–China technical discussion. The authors would also like to thank Dr. H. Sun for his support while he was the Facility Manager of the research group.

References

[1] R. W. Shaffer, "Chapter 12: Scroll compressors," in *Compressor Handbook*, Paul C. Hanlon, Ed. New York, NY, USA: McGraw-Hill, 2001.

[2] Y. Chen, N. P. Halm, E. A. Groll, and J. E. Braun, "Mathematical modeling of scroll compressors—Part I: Compression process modeling," *Int. J. Refrig.*, vol. 25, no. 6, pp. 731–750, Sep. 2002.

[3] Compressed air batteries, Flow battery Ltd., 2012. [Online]. Available: http://www.flowbattery.co.uk/compressed-air-batteries. Accessed on: Jan. 16, 2016.
[4] X. Luo, H. Sun, and J. Wang, "An energy efficient pneumatic-electrical system and control strategy development," in *Proc. Amer. Control Conf.*, 2011, pp. 4743–4748.
[5] J. Wang *et al.*, "Mathematical modeling study of scroll air motors and energy efficiency analysis—Part II," *IEEE/ASME Trans. Mechatronics*, vol. 16, no. 1, pp. 122–132, Feb. 2011.
[6] T. Yanagisawa, Y. Fukuta, T. Ogi, and T. Hikichi, "Performance of an oil-free scroll-type air expander," in *Proc. ImechE Conf. Trans Compressors Their Syst.*, 2001, pp. 167–174.
[7] P. Song, M. Wei, L. Shi, S. N. Danish, and C. Ma, "A review of scroll expanders for organic Rankine cycle systems," *Appl. Therm. Eng.*, vol. 75, pp. 54–64, Jan. 2015.
[8] J. Wang, L. Yang, X. Luo, S. Mangan, and J. W. Derby, "Mathematical modeling study of scroll air motors and energy efficiency analysis—Part I," *IEEE/ASME Trans. Mechatronics*, vol. 16, no. 1, pp. 112–121, Feb. 2011.
[9] R. Dickes, "Design and fabrication of a variable wall thickness two-stage scroll expander to be integrated in a micro-solar power plant," M.S. thesis, Dept. Aero. Mech. Eng., Univ. Liége, Liège, Belgium, 2013.
[10] M. Wei, P. Song, B. Zhao, L. Shi, Z. Wang, and C. Ma, "Unsteady flow in the suction process of a scroll expander for an ORC waste heat recovery system," *Appl. Therm. Eng.*, vol. 78, pp. 460–470, Mar. 2015.
[11] X. Gao, L. S. Li, Y. Zhao, P. C. Shu, and J. Shen, "Research on a scroll expander used for recovering work in a fuel cell," *Int. J. Thermodyn.*, vol. 7, no. 1, pp. 1–8, Mar. 2004.
[12] X. Luo, J. Wang, H. Sun, J. W. Derby, and S. J. Mangan, "Study of a new strategy for pneumatic actuator system energy efficiency improvement via the scroll expander technology," *IEEE/ASME Trans. Mechatronics*, vol. 18, no. 5, pp. 1508–1518, Oct. 2013.
[13] X. Luo, J. Wang, C. Krupke, and H. Xu, "Feasibility study of a scroll expander for recycling low-pressure exhaust gas energy from a vehicle gasoline engine system," *Energies*, vol. 9, no. 4, 2016, doi: 10.3390/en9040231.
[14] C. Krupke, J. Wang, J. Clarke, and X. Luo, "Modeling and experimental study of a wind turbine system in hybrid connection with compressed air energy storage," *IEEE Trans. Energy Convers.*, vol. 32, no. 1, pp. 137–145, Mar. 2017.
[15] L. Varriale, Compressed air battery, 2012. [Online]. Available: https://www.bestmag.co.uk/tags/compressed-air-battery. Accessed on: Jul. 20, 2016.
[16] Affordable domestic microCHP boiler, 2014. [Online]. Available: http://flowgroup.uk.com/. Accessed on: Nov. 20, 2016.
[17] Airsquared scroll expander products and projects, 2011. [Online]. Available: https://airsquared.com/products/scroll-expanders/. Accessed on: Jun. 12, 2017.
[18] "Rear-earth permanent magnets VACODYM and VACOMAX," Product brochure, VACUUMSCHMELZE GmbH & Co. KG, 2014. [Online]. Available: http://www.vacuumschmelze.com/en/products/permanent-magnets-assemblies.html. Accessed on: May 26, 2016.
[19] X. Luo, H. Sun, and J. Wang, "A novel magnetic scroll expander as a drive for electricity generation," in *Proc. 7th IET Int. Conf. Power Electron. Mach. Drives*, 2014, pp. 1–6.
[20] J. Wang, J. Pu, J. P. Moore, and Z. Zhang, "Modelling study and servo-control of air motor systems," *Int. J. Control*, vol. 71, no. 3, pp. 459–476, 1998.
[21] Y. Katano, K. Nakano, M. Otsuki, and H. Matsukawa, "Novel friction law for the static friction force based on local precursor slipping," *Scientific Reports*, vol. 4, no. 6324, 2014. [Online]. Available: http://www.nature.com/articles/srep06324. Accessed on: Apr. 16, 2016.
[22] B. Armstrong-Helouvry, P. Dupont, and C. C. Dewit, "A surrey of models analysis tools and compensation methods for the control of machines with friction," *Automatica*, vol. 30, pp. 1083–1138, 1994.
[23] J. Gravesen and C. Henriksen, "The geometry of the scroll compressor," *SIAM Rev.*, vol. 43, pp. 113–126, 2001.
[24] W. H. Hayt, Jr., and J. A. Buck, *Engineering Electromagnetics*, 7th ed. New York, NY, USA: McGraw-Hill, 2006, pp. 290–305.
[25] P. A. Watterson, "Energy calculation of a permanent magnet system by surface and flux integrals (the flux-mmf method)," *IEEE Trans. Magn.*, vol. 36, no. 2, pp. 470–475, Aug. 2000.
[26] H. C. Lovatt and P. A. Watterson, "Energy stored in permanent magnets," *IEEE Trans. Magn.*, vol. 35, no. 1, pp. 505–507, Jan. 1999.
[27] X. Q. Li and J. Wang, "Influence of axial clearance of orbiting scroll on working performance of scroll compressor," *J. Compressor Technol.*, vol. 1, pp. 23–26, 2007.
[28] Z. L. Gu, Y. Z. Yu, and S. Y. Feng, Eds. *Scroll Compressors and Scroll Mechanics*. Xi'an, China: Shaanxi Sci. Technol. Press, 1998.
[29] T. D. Eastop and A. McConkey, *Applied Thermodynamics for Engineering Technologists*. Singapore: Longman, 1993, pp. 20–56, 115–121.
[30] M. Cai, K. Kawashima, and T. Kagawa, "Power assessment of flowing compressed air," *Trans. ASME J. Fluids Eng.*, vol. 128, pp. 402–405, 2006
[31] M. Cai, T. Kaawa, and K. Kawashima, "Energy conversion mechanics and power evaluation of compressible fluid in pneumatic actuator systems," presented at the 37th Intersoc. Energy Convers. Eng. Conf., Washington, DC, USA, 2002.

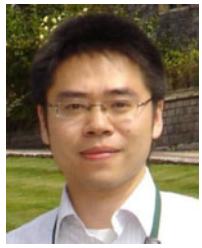

Xing Luo received the M.Sc. degree in microelectronic systems and telecommunications from the University of Liverpool, Liverpool, U.K., in 2006, and the Ph.D. degree in mechatronics from the University of Birmingham, Birmingham, U.K., in 2010.

He is currently a Senior Research Fellow of energy conversion and control engineering with the School of Engineering, University of Warwick, Coventry, U.K. His current research interests include system modeling and control on electrical energy storage, power systems, vehicle and pneumatic systems, hardware-in-the-loop simulation, energy-efficient systems, and real-time control development.

Jihong Wang (M'06–SM'08) received the B.E. degree from the Wuhan University of Technology, Wuhan, China, in 1982, the M.Sc. degree from the Shandong University of Science and Technology, Shandong, China, in 1985, and the Ph.D. degree from Coventry University, Coventry, U.K., in 1995.

She is currently a Professor of power systems and control engineering with the School of Engineering, University of Warwick, Coventry. Her current research interests include nonlinear system control, system modeling and identification, power systems, energy-efficient actuators and systems, and applications of intelligent algorithms.

Dr. Wang was a Technical Editor for the IEEE TRANSACTIONS ON MECHATRONICS.

Leonid Shpanin (M'08) received the Ph.D. degree in electrical and electronic engineering from the University of Liverpool, Liverpool, U.K., in 2006.

He is currently a Lecturer in aerospace with the Faculty of Engineering, Environment, and Computing, Coventry University, Coventry, U.K. He has over ten years of industrial experience in electrical/electronic engineering and radio frequency communication systems where he was involved in the variety of research, engineering, and management positions in the U.K. and across the world. His current research interests include pulsed power systems, high voltage dc circuit breakers, renewable energy systems, unmanned aerial vehicle energy management systems, and power systems modeling and control.

Mark Dooner received the M.Eng. degree in electronic engineering and the Ph.D. degree in automotive mechatronics from the University of Warwick, Coventry, U.K., in 2011 and 2017, respectively.

He is a Research Fellow with the Power and Control Systems Research Laboratory, University of Warwick. His current research interests include energy storage systems modeling and control, electromagnetic modeling, and power systems.